Proceedings of Zurich 2018
Global Power and Propulsion Forum
10th January – 12th January, 2018
http://www.gpps.global

GPPS-2018-0016

INFLUENCE OF AERODYNAMIC DAMPING ON TORSIONAL VIBRATIONS OF TURBINE SHAFTS

Christopher E. Meinzer*
Christian Keller
Graduate Research Assistants
Joerg R. Seume
Professor
Institute of Turbomachinery
and Fluid Dynamics
Faculty of Mechanical Engineering
Leibniz Universität Hannover
30167, Hannover, Germany

Olga Korolova
Graduate Research Assistant
Bernd Ponick
Professor
Institute for Drive Systems
and Power Electronics
Faculty of Electrical Engineering
and Computer Science
Leibniz Universität Hannover
30167, Hannover, Germany

ABSTRACT

Since the early seventies, the excitation of torsional vibrations of turbine shafts of large fossil and nuclear power plants has been addressed in research. In the past, grid-induced instabilities in long transmission lines, e.g., sub-synchronous resonance, and super-synchronous excitation due to the interaction with large nearby consumers were an issue. Today, the rapid transformation from fossil and nuclear multi-megawatt power plants to renewable energy sources and the wide use of frequency inverters hold new challenges.
Hence, grid simulation becomes increasingly important. For such a grid simulation, an electromechanical model of a turbine is presented in this paper. The model includes aerodynamic damping effects of the fluid surrounding the turbine blades. For this a parameter study using a time-linearized CFD with mesh motion is executed and a damping model is derived from the data. The aerodynamic damping forces acting on the turbine blades can have a significant effect on the models response when the rotor shaft is excited by line-to-line shorts in the turbine generator.

NOMENCLATURE

C	Damping matrix
E_{modal}	Modal energy of blade vibration
J	Inertia matrix
K	Stiffness matrix
Λ	Log. decrement of aerodynamic damping
L	Inductance matrix
m	Electromagnetic torque
M	Torque vector
$\dot{m}$	Mass flow rate
$\dot{m}_{red}$	Reduced mass flow rate
$\dot{m}_{adp}$	Design point $\dot{m}$
n	Rotational speed
n_{red}	Reduced rotational speed
P_{tot}	Total pressure
$P_{tot,adp}$	Design point P_{tot}
ϕ	Rotor position
R	Resistance matrix
T_{tot}	Total temperature
W_{cyc}	Work per cycle
ω	Rotational speed

1 Introduction

Torsional vibrations of turbine shafts can be excited by harmonic content in the power grid that causes an oscillating torque at the generator. This excitation may eventually lead to high-cycle fatigue (HCF) of rotor components, that exhibit resonant eigenmodes in the range of this excitation, including but not limited to the long and slender blades of the low-pressure stages of the turbine. In the literature, several of such cases are documented. A comprehensive report by the Electric Power Research Institute lists 12 cases alone in which grid-induced excitation of

*Address all correspondence to this author, meinzer@tfd.uni-hannover.de.

torsional vibrations led to significant damage of shafts, blades and generators (Walker, Giesecke, and Stein (2005)). Further incidents are reported by Bovsunovsky (2015), Okabe et al. (2012), and Reid and Lewis (2012).

Research on the interaction of the mechanical system with the electrical grid commenced after the consecutive failure of two shafts at the Mohave Generating Station in Nevada in 1971 and the following investigations. Resonance phenomena in the electrical grid had already been known and researched for a number of decades before, however the implications for the mechanical system were overlooked, because the phenomena were perceived to be of solely electrical interest (Walker et al. (1975)). At Mohave, an electrical resonant frequency of the grid excited a torsional mode of the rotor at 30 Hz, resulting in high vibration amplitudes in the shaft section between generator and exciter. This eventually caused fatigue cracks in the rotor, as well as an electrical ground due to failure of the electrical insulation, resulting in electrical arcing and the burning of the rotor (Walker, Giesecke, and Stein (2005)).

In another incident a retainer ring, which held the coils near the end winding on the generator rotor, failed in early 1993 at Comanche Unit 2, a 335 MW coal-fired power plant in Colorado. Here, an exciter was replaced after 18 years of operation. The temporarily installed exciter moved a torsional mode from a frequency of 120.9 Hz to 118 Hz that just a few years earlier had been tuned away from 120 Hz to avoid excitation by negative phase sequence currents. Unfortunately, the new exciter led to a change of the mode shape of the rotor train, which then exhibited much larger torsional amplitudes at the retainer ring. The grid-induced excitation is particularly interesting at this site, because the power plant neighbors a steel mill with a power usage of 100 MW. The investigation following the incident showed that the power factor regulator of the steel mill's Static var Flicker Controller with the seventh and/or sixth harmonic filter off-line became unstable at low load conditions at the steel mill, directly causing high vibration in the generator (Dorfman et al. (1996)).

In 2002, blades in a low-pressure turbine of Unit 2 of the South Texas Nuclear Project power plant were found to have cracked due to high cycle fatigue. The generator was slightly changed, increasing the power by 1.4%. This was encompassed by some repair work done to coil slots that were machined incorrectly during the upgrade. However small these changes seemed, they tuned a rotor torsional mode into close proximity of 120 Hz, twice the line frequency, at which negative phase sequence currents excite the rotor in normal operation (Halpin (2003)).

The technical community reacted to this with the introduction of the ISO 22266-1:2009 norm, which provides frequency ranges to designers in which an excitation is to be expected and subsequently torsional shaft modes must be avoided. Moreover, the norm describes measurement techniques to identify torsional vibrations in shop and on-site tests. Using these test, the mandatory calculation can be validated for the specific turbine build and hence a reduced frequency margin is allowable. If no torsional mode is found within the primary frequency exclusion zone (PFEZ), no further testing is required. The PFEZ is recommended as a $\pm$ 6% margin around the line frequency, and twice the line frequency (ISO 22266-1:2009).

The operating conditions and faults that lead to typical disturbances in the electrical grid relevant to the excitation of torsional vibrations are summarized in ISO 22266-1:2009. In steady-state operation, line and load unbalances can lead to a super-synchronous excitation at twice the line frequency. Subsynchronous resonance (SSR) can cause an excitation below the line frequency in both steady and transient operation. SSR refers to an instability found in long transmission lines with series compensating capacitors installed to decrease the otherwise high inductive reactance (Walker, Giesecke, and Stein (2005)). Transient disturbances that excite at twice the line frequency are unbalanced shorts (line to line and line to ground), single pole switching, and disturbances in the grid due to control devices. At line frequency, out-of-phase synchronization, grid disturbances and switching become relevant. Short circuits, pole switching and faulty synchronization impose a step change to the system that excites a broader range of frequencies (ISO 22266-1:2009).

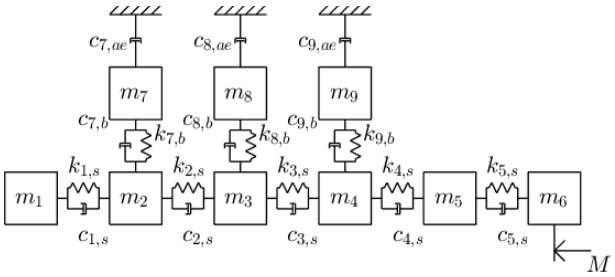

FIGURE 1: Lumped-mass model of the rotor

Grid disturbances due to control devices such as DC power converters at industrial sites, connections of AC transmission lines with HVDC transmission lines, and turbines connected directly to HVDC transmission lines are summarized by the term Device Dependent Sub-synchronous Oscillations DDSO (Walker, Giesecke, and Stein (2005)). This includes variable-frequency electric drives used in power plant sub systems, or in industrial plants in close electrical proximity.

In the light of the rapid transformation from fossil and nuclear multi-megawatt power plants to renewable energy sources, new challenges arise. The number of grid feed-in points increases, especially on sub-transmission levels, e.g., low and medium-voltage level, as does the number of participants (Rudion et al. (2006)). Moreover, in this scenario of distributed generation, the producers and consumers will not only be situated in closer proximity to each other, but will also be of more equal power, as the input power of the distributed generation units is much lower. With the rapid increase of distributed generation, the need to simulate such distribution networks rises.

The objective of this paper is to provide a method to model torsional vibration of turbine shafts with the inclusion of aerodynamic damping effects for such grid simulations. The mechanical model includes the rotor shaft, blades and the generator and only torsional vibrations of the shaft are considered. The main challenge is the development of an aerodynamic damping model suitable for simple inclusion based on scaling damping coefficients of a known design. The influence of the added aerodynamic damping are investigated simulating a line-to-line short.

2 Coupled Blade-Shaft Torsional Vibration

The torsional vibration behavior of shafts is studied in rotor dynamics. The blades attached to the rotor are usually modeled as rigid bodies or mass points, which add to the overall inertia of the respective shaft section. During the aeromechanical blade design, the blade is either fixed at the blade root, or attached to the flexible disk to allow interblade coupling, but the shaft is assumed to be rigid. However, both modeling approaches fall short for the torsional vibration phenomena discussed above.

The number of interactions which may lead to resonance between shaft and blade is limited by kinematic constraints. For a shaft torsional vibration, a coupling is possible with tangential blade vibrations. In this case, all blades have to vibrate in phase so that the blade assembly has zero nodal diameters. Every other case is not coupled. For axial shaft vibrations, a similar observation holds, in that blades have to perform an axial motion with all blades in phase, again having a nodal diameter of 0. For shaft bending motions, a coupling with the blade assembly vibrating with one nodal diameter is possible (opposite blades are vibrating 180° out of phase). More details and a complete overview are given by Okabe et al. (2012). Since only torsional shaft vibrations are relevant in the context of grid induces vibrations, the coupling is limited to only one possible interaction.

Depending on the problem at hand, different methods exist to study these coupled vibrations. The simplest method is a lumped-mass model, which has been previously used by Hammons (1980) and Liu, Jiang, and Chen (2014). If more accuracy is needed, continuum modeling using finite elements (FEM) can be used (Gonzalez et al. (1984) and Liu, Jiang, and Chen (2014)). These FEM models consist of several thousands to millions of degrees-of-freedom (DOF), which is time consuming to solve and an inclusion in a transient grid simulation might become prohibitively computationally expensive. To reduce complexity, reduced-order models can be derived from the FEM models, thus reducing the number of DOF (Okabe et al. (1991)).

In this study, the lumped-mass model approach is implemented, because the turbine model discussed in Sec. 3 is to be integrated in a grid simulator. The objectives of this study are: 1. to derive a model for the aerodynamic damping of the blades using a CFD parameter study, 2. to build a lumped-mass turbine model that includes the aerodynamic damping model, and 3. to examine the effects of aerodynamic damping on the systems response.

3 Turbine Model

With the performance limitations of the grid simulation in mind, the turbine is modeled as a lumped-mass model with branches for the blade rows. The shaft sections are modeled with their respective inertia and torsional stiffness, and the blades of each row are modeled as a mass coupled to the respective shaft section with a spring and damper. To estimate the stiffness of the spring, a beam of the blades' length and cross-section is used. The blade row masses are connected to the frame of reference by dampers representing damping of the surrounding fluid in the turbine, see fig. 1.

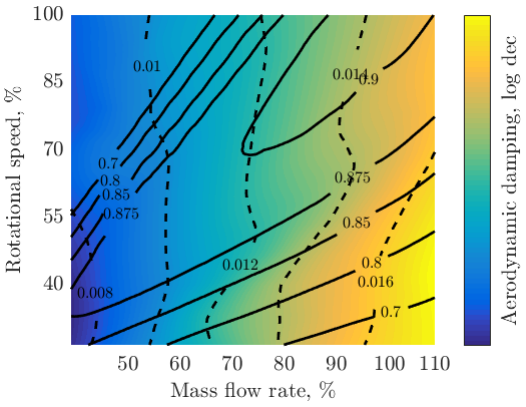

FIGURE 2: Aerodynamic damping (log dec) for ND 0, solid lines show isentropic efficiency

3.1 Aerodynamic Damping Model

The aerodynamic damping of a turbine blade is highly dependent on the fluid properties, e.g., flow velocity, flow incidence, pressure, and temperature. Furthermore, the mode shape, the phase-lag to the neighboring blade (interblade phase angle, IBPA), and the frequency at which the blade oscillates highly impact the aerodynamic damping. In fact, the aerodynamic damping can even become negative, resulting in a self-excited vibration referred to as flutter, which potentially leads to high-cycle fatigue damage and eventually blade loss if the turbine is not shut down fast enough. The aerodynamic damping, represented by the logarithmic decrement, is calculated from the ratio of the real part of the unsteady work per cycle to the in-vacuo vibration energy of that mode Kersken et al. (2010)

$$\Lambda = \frac{\Re(W_{cyc})}{2E_{modal}}. \tag{1}$$

The cyclic work itself is given by Kersken et al. (2010) as

$$W_{cyc} = -i\pi \int_{\Gamma} \tilde{\mathbf{x}}^{H} (\tilde{p}\mathbf{n}^{0} + p^{0}\tilde{\mathbf{n}}) dS, \tag{2}$$

with $\tilde{\mathbf{x}}$ as the complex mode shape, $\tilde{p}$ the complex unsteady pressure, $\tilde{\mathbf{n}}$ the normal vector on the blade surface. As Kielb et al. (2006) show, the term $p^{0}\tilde{\mathbf{n}}$ will vanish for real mode shapes, such as a vibration with nodal diameter zero. At nodal diameter zero all blades vibrate in-phase; hence this nodal diameter is prone to be excited by torsional vibration of the shaft. To develop a model of reduced complexity, which estimates the aerodynamic damping, a parametric study using computational fluid dynamics (CFD) is performed with the following limiting assumptions: absence of shocks and large flow separations, and positive damping for all IBPA.

For the parametric study, a low cambered turbine profile (Meinzer et al. (2015)) is used. The CFD analysis is executed using the Reynolds-averaged Navier-Stokes (RANS) solver TRACE (Becker, Heitkamp, and Kügeler (2010)) with the time-linearized aeroelasticity module described by Kersken et al.

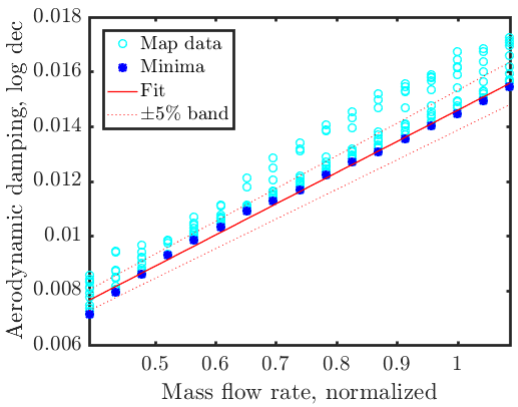

FIGURE 3: Aerodynamic damping (log dec) over mass flow rate, solid line represents a linear fit of the respective minima

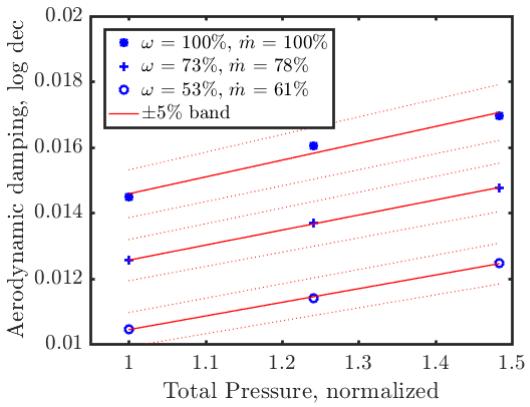

FIGURE 4: Aerodynamic damping (log dec) for higher total pressure levels

(2010). TRACE is a turbomachinery specific CFD code, which is developed by the German Aerospace Center (DLR). This solver is used for turbomachinery research at a number of universities throughout Germany and in the turbomachinery industry. Turbulence is modeled using the $k-\omega$-Model with a low-Reynolds grid and y+ ≈ 1. For the steady flow solution, a grid study on the pressure ratio was performed before the time-linearized simulations, because it relies on a steady RANS start solution and the pressure is the relevant flow parameter used in the calculation of aerodynamic damping (Eq. 2). The grid convergence indices are $GCI_1 = 0.016125\%$, $GCI_2 = 0.059307\%$, and $GCI_3 = 0.2182\%$. Due to the large number of simulations performed, the coarse grid (no. 3) is used for the parametric study for both the steady RANS and the time-linearized solution.

In Fig. 2, the aerodynamic damping as a logarithmic decrement, for the relevant nodal diameter of zero (IBPA 0 deg) is shown over a range of rotational speeds and mass flow rates, with respect to the aerodynamic design point of the turbine. This suggests that for the nodal diameter zero, where all blades vibrate inphase and which is the nodal diameter that is excited by torsional vibration of the rotor shaft, aerodynamic damping is almost constant over the rotational speed. If the rotational speed changes at constant mass flow rate and thus constant axial flow velocity, the flow incidence changes. Likewise a change mass flow rate at a constant speed changes the flow incidence. This can be observed in Fig. 2 by looking at the solid lines which show constant isentropic efficiency. A high efficiency is encompassed by low flow incidence and little or no flow separation. The dashed contour lines, which show the aerodynamic damping, are almost independent of the rotational speed.

The dependence of the aerodynamic damping on the mass flow rate, which determines the axial flow velocity, is shown in Fig. 3. A linear trend of the aerodynamic damping for all rotational speeds with respect to the mass flow rate is observed. A conservative damping estimate can be established by a linear fit of the minimum aerodynamic damping. To include the effects of an increase in pressure, for example when looking at another turbine stage, the pressure level was increased for three operating points. As this also means a change in temperature and density, the reduced mass flow rate $\dot{m}_{red}$ and the reduced rotational speed n_{red} are kept constant:

$$\dot{m}_{red} = \frac{\dot{m} p_{Ref}}{p_{tot,inlet}} \sqrt{\frac{T_{tot,inlet}}{T_{Ref}}} \tag{3}$$

$$n_{red} = n \sqrt{\frac{T_{tot,inlet}}{T_{Ref}}} \tag{4}$$

This ensures Mach-number similarity. Hence, the flow angles and the incidence are preserved. The change of aerodynamic damping with the pressure level is depicted in Fig. 4. It can be observed that all three operating points support a linear trend of a similar slope. Within the investigated range, the influence of mass flow rate and pressure were found to be decoupled. The impact of temperature on the Young's-modulus of the blades is omitted here.

Within the limits stated above, a model for the aerodynamic damping in form of the logarithmic decrement (Λ) as a function of mass flow ratio and pressure level can be derived for this turbine by fitting the numerical data:

$$\Lambda = 0.01141 \left(\frac{\dot{m}}{\dot{m}_{adp}} \right) + 0.003091 \left(\frac{p_{tot}}{p_{tot,adp}} - 1 \right) + 0.003168. \tag{5}$$

A comparison of the damping model (Eq. 5) with CFD results for operating point $\omega = 87\%, \dot{m} = 87\%$ is shown in Fig. 5.

The linear character of the aerodynamic damping with pressure has been shown by other authors as well, c.f. Kammerer and Abhari (2009). For the example above, the increase in mass flow rate results from a larger pressure difference over the turbine, which also influences aerodynamic damping. Even though the derived damping model represents the examined turbine quite satisfactory, a transfer to other turbines entails additional simulations. An a priori estimate for an arbitrary blade is not possible, since the aerodynamic damping is sensitive to the mode shape, the eigenfrequency of the blade, and the steady aerodynamics. The latter is governed by the blade geometry, which again influences mode shape and eigenfrequency. To adapt this model to

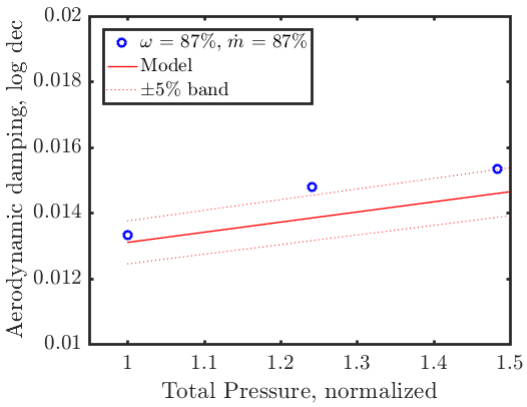

FIGURE 5: Comparison of the damping model (Eq. 5) with CFD results for operating point $\omega = 87\%, \dot{m} = 87\%$

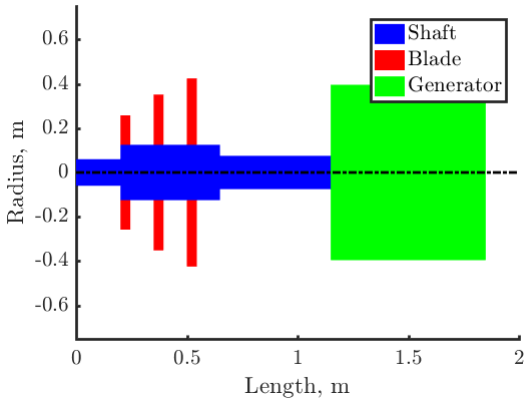

FIGURE 6: Sketch of the rotor model

other blades, the slope of the damping curve would need to be corrected. In most cases, the required data for this will already be available from turbine design. With large amplitudes and in the presence of shocks it is likely that the aerodynamic damping will divert from its linear character.

3.2 Mechanical Model

Turbine shafts experience lateral, axial, and torsional vibration when rotating. The lateral and axial vibrations are subject to significant damping in the oil bearings while the torsional vibration have almost no damping. This suggests that the aerodynamic damping of the rotor blades may have an influence on torsional shaft vibrations. As mentioned above, the tangential component of blade motion will add to the torsional motion of the shaft only when all blades oscillate with no phase-lag to each other (nodal diameter zero). The axial component of such a mode (umbrella mode) would add to the axial shaft motion, while a nodal diameter one mode of the blade assembly (i.e. upper half of the blades moves in the opposite direction of the lower half of the blades) would couple to a lateral shaft mode. For all other blade modes, the forcing on the shaft motion is canceled out. This observation reduces the DOF of the problem drastically.

The turbine model herein consists of shaft sections and blade sections as depicted in Fig. 6, which shows a sketch of the turbine. The shaft sections are defined by radius and length, together with the material properties density, Young's modulus, and Poisson ratio. Both inertia and torsional stiffness are calculated from the shaft's properties. For material damping a typical damping is assumed. All data is found in Tab. 1. With this, the parameters for the equation of motion Eq. 6 are defined:

$$\mathbf{J}\ddot{\omega} + \mathbf{C}\dot{\omega} + \mathbf{K}\omega = \mathbf{M}. \tag{6}$$

Each shaft section is defined by it's inertia, a stiffness, and a mechanical damping coefficient. The blades are coupled to the respective shaft sections via the stiffness $\mathbf{K}$ and damping matrix $\mathbf{C}$ and to the frame of reference with the aerodynamic damping coefficient given by the model Eq. 5. $\mathbf{M}$ denotes the torque vector. The structure of the lumped-mass model can be seen from the damping matrix $\mathbf{C}$ given in appendix A and in Fig. 1. For the present case the blades' eigenfrequencies are tuned in such a way that the last blade row vibrates at the line frequency and the middle blade row at twice the line frequency, while the mass flow rate is varied at 100%, 78%, and 61%, of the nominal mass flow rate.

TABLE 1: Material properties

Name	Unit	Value
Density	kg/m^3	7850
Young's modulus	Pa	2.059E11
Poisson ratio	-	0.3
Material damping	log. dec.	0.0001

3.3 Influence of Aerodynamic Damping

The aerodynamic damping of $\approx 1\%$ derived from the simulation above and incorporated in the model is of the order of magnitude measured by Rice, Bell, and Singh (2009) on a final stage steam turbine blade. In technical applications, damping is beneficial if it limits the amplitude vibrating structures which otherwise would be exposed to a higher dynamic load. To judge the influence of the aerodynamic damping, it is notable that in turbomachines it is of the order of the friction damping present in the blade root joint, rather than of the order of the almost negligible material damping. On this account, the consideration of aerodynamic damping may add another degree of freedom in the design process, because the operating margin can potentially be extended. This of course requires a well-validated code for aeroelastic simulation to feed the above model with damping coefficients for the specific design. In the case of zero nodal diameter excitation, the aerodynamic damping adds a positive damping to the system. Hence, omitting it and choosing a lower than ac-

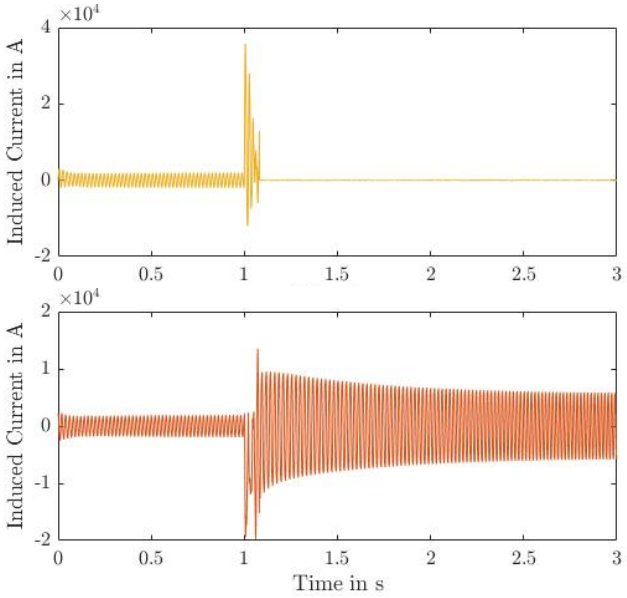

FIGURE 7: Currents induced in line 3 without short (top) and line 2 (bottom), which is shorted to line 1

tual friction damping will lead to a more conservative amplitude estimation, but will leave this design potential unexploited. Figure 2 shows that in the present case the aerodynamic damping is rather independent of the rotational speed of the rotor. The friction damping in the blade root will decrease with the rotational speed because the increasing centrifugal force reduces the motion in the blade root joint. Thus, the aerodynamic damping will compensate the lack of damping at high rotational speeds of the rotor.

4 Generator Model

A synchronous generator is part of the system studied and its model has to be connected to the turbine model via the common state variables for the dynamical simulation. Thus the interaction between the mechanical the electromagnetic subsystems is realized through the inner electromagnetic torque M_i of the generator and the rotational speed ω_m of the rotor shaft.

Two different dynamical models of the generator were developed and integrated into the system in order to study its dynamics with and without considering the higher spatial harmonic effects. The former generator model was developed formulating the differential equations of the electromagnetic subsystem in a two-axis reference frame attached to the rotor with the state space vector $\mathbf{i} = [i_\mathrm{d}, i_\mathrm{q}, i_\mathrm{fd}, i_\mathrm{Dd}, i_\mathrm{Dq}]$ where i_d, i_q, i_Dd and i_Dd are the stator and rotor damping cage current components respectively, obtained with the Park transformation, and i_fd is the rotor excitation current.

The latter model is aimed at simulating the effect of the higher spatial harmonics in the magnetic field of the air-gap which excite oscillations in the electromagnetic system and subsequently in the inner electromagnetic torque of the generator . Therefor the differential equations describing the electromagnetic subsystem were formulated in the stationary reference frame with a state space vector $\mathbf{i} = [i_1, i_2, i_3, i_\mathrm{fd}, i_\mathrm{Dd}, i_\mathrm{Dq}]$ where i_1,i_2,i_3 are the currents in the stator strands (lines 1-3). Both for presentation and simulation it is convenient to express these differential equations in the following matrix form

$$\frac{d\mathbf{i}}{dt} = \mathbf{L}^{-1}(\gamma)\cdot(-\mathbf{R} - \frac{\partial \mathbf{L}(\gamma)}{\partial \gamma} p\omega_\mathrm{m})\mathbf{i} + \mathbf{L}(\gamma)^{-1}\mathbf{u} \tag{7}$$

$$m_\mathrm{i} = \frac{1}{2} p \mathbf{i}^\mathrm{T} \frac{\partial \mathbf{L}(\gamma)}{\partial \gamma}\mathbf{i}, \tag{8}$$

where $\mathbf{L}(\gamma)$ is the inductance matrix, $\mathbf{R}$ is the resistance matrix, p is the number of pole pairs of the generator and γ is the rotor position.

5 Results

As a proof of concept and in order to investigate the influence of added aerodynamic damping on the vibration amplitude and total damping, the grid simulator is run using one operation scenario for a variation of parameters with and without aerodynamic damping. In the scenario, the model is first run until a steady state is reached. At this point, a line to line short occurs between two poles. After 80 ms the generator is disconnected from the grid. As a simplification, the torque is kept at a constant level, which causes the shaft to accelerate. This way the overall damping and maximum amplitude can be calculated more reliably and can be compared with each other. In a real world scenario, the mass flow to the turbine would be cut off after the generator is disconnected from the grid, so there is no external torque.

The scenario is investigated for the shaft configuration described above at 61%, 78% and 100% nominal mass flow with and without aerodynamic damping. Because rotor speed has only a small influence on aerodynamic damping, it is kept constant. In order to explain what happens after the short, the stator currents of line 3, which is not shorted to another line, and line 2, which is shorted to line 1, are plotted in Fig. 7. The system is started with almost stable initial conditions and approaches stable operation at $t = 1\ s$. At this moment, a short between lines 1 and 2 is introduced, causing an abrupt spike in current in all lines. After disconnecting the generator from the grid, current in line 3 rapidly goes to zero, since there cannot be a net current without violating continuity. In lines 1 and 2, a current continues to be induced after the separation, which may lead to additional damage to the generator or even the rotor due to the high resulting shaft vibrations.

The rotor reacts to the short with a relatively high amplitude of vibration that afterwards decays exponentially. From this, two results can be obtained: the maximum amplitude of vibration right after the short and the rate of exponential decay, from which an overall damping can be computed. Figure 8 shows the relative movement of the blades of the last stage with respect to the generator. The drift is due to the rotor spinning up.

The vibration of a damped harmonic oscillator can be described by

$$x(t) = ae^{\lambda t} \tag{9}$$

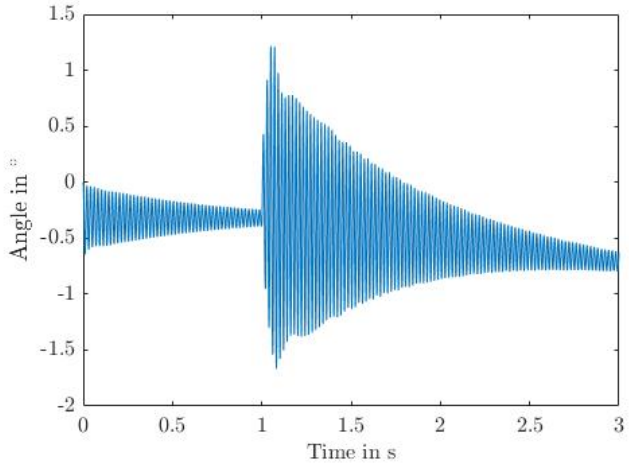

FIGURE 8: Response of the last stage to a two-pole short circuit

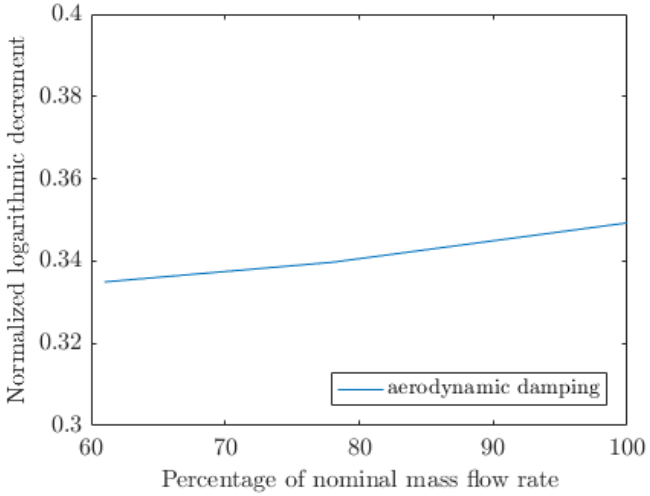

FIGURE 9: Normalized total logarithmic decrement with and without aerodynamic damping

with

$$\lambda = -\omega_n(\zeta \pm i\sqrt{1-\zeta^2}) = b + ic \tag{10}$$

in which ζ is the damping ratio and ω_n is the eigenfrequency of the component. The real part b of the exponent λ describes the decay of the vibration amplitude due to damping, while the imaginary part c describes the harmonic oscillation. The real part of eqn. (9) can be used to fit the exponential decay of the blade or shaft vibration. There are several possibilities to extract the decay rate from data such as those shown in Fig. 8. A simple method would be to determine the envelope by determining all maxima (or minima) and finally applying an exponential fit to these points. This approach may be sensitive to disturbances overlying the harmonic response, which can negatively impact the quality of the fit. A more elegant method is to apply a wavelet transformation (Carassale, Marrè-Brunenghi, and Patrone (2018)) to the data along a fixed frequency. With a properly adjusted wavelet, the time dependent amplitude of vibration at a specific frequency can be very accurately defined, resulting in exponential least squares fits with a value of 1 for R^2.

With the damping ratio identified, the logarithmic decrement can be obtained via $\Lambda = 2\pi\zeta$ for small damping values. All results are normalized with respect to the case with no aerodynamic damping and a mass flow rate of 100%. In order to interpret the results truthfully, one has to keep in mind that aerodynamic damping and damping at the joint between blade and disk/shaft are of roughly the same order of magnitude. Furthermore, the case investigated serves mainly as a means to quantify the relative influence of aerodynamic damping in this specific configuration.

Figure 9 shows the total normalized logarithmic decrement for the last stage as derived from its vibration response. Overall, damping increases by approximately 35% with the introduction of aerodynamic damping and is higher for higher mass flow rates. Results appear to be plausible, since damping stays the same for all mass flow rates if no aerodynamic damping is applied.

While overall damping is an indicator of the systems dynamic response, the resulting maximum amplitude of vibration may be of more practical relevance. In Fig. 10 the normalized maximum amplitude is shown again with and without aerodynamic damping for varying mass flow rates. The maximum response amplitude with aerodynamic damping is offset from the maximum amplitude without aerodynamic damping by a roughly constant negative value. On average, the amplitude decreases by approximately 3.7% under the influence of aerodynamic damping. Even though the change in overall damping is quite large, the effect on the maximum response is comparatively low.

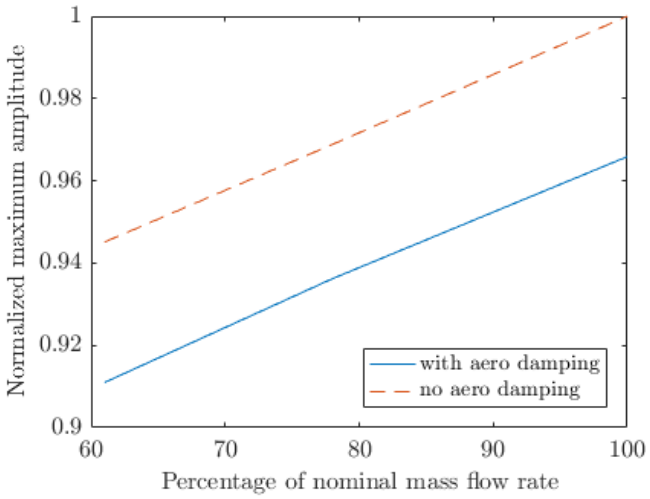

FIGURE 10: Normalized maximum response amplitude with and without aerodynamic damping

6 Conclusions

In this paper, a mechanical lumped-mass model of a turbine shaft including a generator and aerodynamic damping for the simulation of grid-induced torsional vibrations has been introduced. Several simplifications could be made, including the lim-

itation to only one coupled nodal diameter for each rotor stage, which dramatically reduces the number of necessary linearized aeroelasticity simulations. Aerodynamic damping was modeled based on extensive CFD-simulations of an axial turbine, from which a relationship between damping and mass flow rate and pressure could be derived. The rotational speed was found to have almost no influence. The combination of the shaft model with the damping model enables its applicability to any operating point inside the normal operating range without shocks or larger flow separations , which are strongly nonlinear flow phenomena. The damping model was verified against additional CFD-simulations. It may not be directly applicable for other turbomachinery configurations, but an adaption should be easily possible in most cases.

The developed turbine model was then coupled to a synchronous generator model, which provides a method for the unsteady simulations of rotor and stator currents and the mechanical response of the system. One specific failure scenario, a two-line short circuit with consecutive separation of the generator from the grid, was investigated in detail in order to quantify the influence of aerodynamic damping on the shaft's vibration. In the configuration presented here, damping at the joints between blades and disk and aerodynamic damping were of the same order of magnitude. Even though aerodynamic damping has a large influence on overall damping, the maximum response amplitude is only reduced by approximately 3.7%. This leads to the conclusion, that an inclusion of aerodynamic damping into the model is likely only beneficial in similar scenarios. In other scenarios, in which aerodynamic damping is very small or friction damping between blade and disk dominates overall damping, an inclusion may not lead to practical benefits. On the other hand it may sometimes be useful to include aerodynamic damping in torsional shaft vibration simulations to be able to achieve a design's full potential.

In the future, the model will be extended to include axial compressors, enabling its application to gas turbines. Furthermore, interactions in a heterogeneous grid will be studied in more detail. Instead of reducing the model a-priori by hand to a lumped-mass representation and tuning it to represent blade and shaft eigenfrequencies, a reduced order model approach could be used to arrive at a model with a similarly small number of degrees of freedom, which offers increased flexibility.

ACKNOWLEDGMENTS

The investigations are conducted as part of the project AMSES "Aggregierte Modelle für die Simulation von dynamischen Vorgängen in elektromechanischen Energiesystemen" (Aggregated models for the simulation of dynamic phenomena in electromechanical energy systems) and within the framework of LiFE 2050, the interdisciplinary research center for the energy sector at Leibniz Universität Hannover, Leibniz Forschungszentrum Energie 2050. The work is supported by the Ministry for Science and Culture of Lower Saxony (Nds. Vorab) under file number ZN3023. Furthermore, the authors thank the DLR Institute of Propulsion Technology for providing TRACE and the Leibniz Universität Hannover IT Services (LUIS) for the computational resources provided.

Appendix A

The structure of the lumped-mass model can be seen from the damping matrix $\mathbf{C}$:

$$\mathbf{C} = \begin{bmatrix} c_{1,s} & -c_{1,s} & 0 & 0 & 0 & 0 & 0 & 0 & 0 \\ -c_{1,s} & c_{1,s}+c_{2,s}+c_{7,b} & -c_{2,s} & 0 & 0 & 0 & -c_{7,b} & 0 & 0 \\ 0 & -c_{2,s} & c_{2,s}+c_{3,s}+c_{8,b} & -c_{s,3} & 0 & 0 & 0 & -c_{8,b} & 0 \\ 0 & 0 & -c_{3,s} & c_{3,s}+c_{s,4}+c_{9,b} & -c_{s,4} & 0 & 0 & 0 & -c_{9,b} \\ 0 & 0 & 0 & -c_{4,s} & c_{4,s}+c_{5,s} & -c_{5,s} & 0 & 0 & 0 \\ 0 & 0 & 0 & 0 & -c_{5,s} & c_{5,s} & 0 & 0 & 0 \\ 0 & -c_{7,b} & 0 & 0 & 0 & 0 & c_{7,b}+c_{7,ae} & 0 & 0 \\ 0 & 0 & -c_{8,b} & 0 & 0 & 0 & 0 & c_{8,b}+c_{8,ae} & 0 \\ 0 & 0 & 0 & -c_{9,b} & 0 & 0 & 0 & 0 & c_{9,b}+c_{9,ae} \end{bmatrix}$$

References

[1] Walker, D., Giesecke, H., and Stein, J. *Steam Turbine-generator Torsional Vibration Interaction With The Electrical Network*. Tech. rep. Electric Power Reserch Institute, 2005.

[2] Bovsunovsky, A. "Fatigue Damage Of Steam Turbine Shaft At Asynchronous Connections Of Turbine Generator To Electrical Network". In: *Journal of Physics: Conference Series*. Vol. 628. 1. IOP Publishing. 2015, p. 012001. DOI: 10.1088/1742-6596/628/1/012001.

[3] Okabe, A., Kudo, T., Shiohata, K., Matsushita, O., Fujiwara, H., Yoda, H., and Sakurai, S. "Reduced Modeling For Turbine Rotor-blade Coupled Bending Vibration Analysis". In: *Journal of Engineering for Gas Turbines and Power* 134.2 (2012), p. 022502. DOI: 10.1115/1.4004145.

[4] Reid, S. R. and Lewis, J. B. “A Resurgence Of Torsional Vibration Concerns For Nuclear And Fossil Steam Turbine Generator Retrofits”. In: *2012 20th International Conference on Nuclear Engineering and the ASME 2012 Power Conference*. ICONE20-POWER2012-55139. American Society of Mechanical Engineers. 2012, pp. 863–867. DOI: 10.1115/ICONE20-POWER2012-55139.

[5] Walker, D., Bowler, C., Jackson, R., and Hodges, D. “Results Of Subsynchronous Resonance Test At Mohave”. In: *IEEE Transactions on Power Apparatus and Systems* 94.5 (1975), pp. 1878–1889. DOI: 10.1109/T-PAS.1975.32034.

[6] Dorfman, L., Riccardella, P., Rosario, D., Sherlock, T., and Stein, J. *Retaining Ring Failure At Comanche Unit 2 TR-106640*. Tech. rep. Electric Power Research Institute, 1996.

[7] Halpin, E. *Turbine Blade Failure - Licensee Event Report 02-004 Supplement*. Tech. rep. South Texas Project Electric Generating Station, 2003.

[8] ISO 22266-1:2009. *Mechanical Vibration - Torsional Vibraion Of Rotating Machinery Part 1: Land-based Steam And Gas Turbine Generator Sets In Excess Of 50MW*. International Organization for Standardization, 2009.

[9] Rudion, K., Orths, A., Styczynski, Z. A., and Strunz, K. “Design Of Benchmark Of Medium Voltage Distribution Network For Investigation Of Dg Integration”. In: *Power Engineering Society General Meeting, 2006. IEEE*. IEEE. 2006, 6–pp. DOI: 10.1109/PES.2006.1709447.

[10] Hammons, T. “Stressing Of Large Turbine-generators At Shaft Couplings And LP Turbine Final-stage Blade Roots Following Clearance Of Grid System Faults And Faulty Synchronisation”. In: *IEEE Transactions on Power Apparatus and Systems* 4 (1980), pp. 1652–1662. DOI: 10.1109/TPAS.1980.319591.

[11] Liu, C., Jiang, D., and Chen, J. “Coupled Torsional Vibration And Fatigue Damage Of Turbine Generator Due To Grid Disturbance”. In: *Journal of Engineering for Gas Turbines and Power* 136.6 (2014), p. 062501. DOI: 10.1115/1.4026214.

[12] Gonzalez, A. J., Kung, G., Raczkowski, C, Taylor, C., and Thonn, D. “Effects Of Single-and Three-pole Switching And High-speed Reclosing On Turbine-generator Shafts And Blades”. In: *IEEE transactions on power apparatus and systems* 11 (1984), pp. 3217–3228. DOI: 10.1109/TPAS.1984.318559.

[13] Okabe, A, Otawara, Y, Kaneko, R, Matsushita, O, and Namura, K. “An Equivalent Reduced Modelling Method And Its Application To Shaft-Blade Coupled Torsional Vibration Analysis Of A Turbine Generator Set”. In: *Proceedings of the Institution of Mechanical Engineers, Part A: Journal of Power and Energy* 205.3 (1991), pp. 173–181. DOI: 10.1243/PIME_PROC_1991_205_026_02.

[14] Kersken, H.-P., Frey, C., Voigt, C., and Ashcroft, G. “Time-linearized And Time-accurate 3d Rans Methods For Aeroelastic Analysis In Turbomachinery”. In: *Proc. ASME Turbo Expo 2010: Power for Land, Sea, and Air*. 2010. DOI: 10.1115/GT2010-22940.

[15] Kielb, R., Barter, J., Chernysheva, O., and Fransson, T. “Flutter Design Of Lowpressure Turbine Blades With Cyclic Symmetric Modes”. In: *Unsteady Aerodynamics, Aeroacoustics and Aeroelasticity of Turbomachines*. Springer, 2006, pp. 41–52.

[16] Meinzer, C. E., Bittner, S. L., Schmitt, S., Kielb, R. E., and Seume, J. R. “Design Of A Single Stage Turbine For The Quantification Of Aerodynamic Damping”. In: *Proc. ASME Turbo Expo 2015: Turbine Technical Conference and Exposition*. GT2015-42641. 2015. DOI: 10.1115/GT2015-42641.

[17] Becker, K., Heitkamp, K., and Kügeler, E. “Recent Progress In A Hybrid-Grid CFD Solver For Turbomachinery Flows”. In: *Proceedings Fifth European Conference on Computational Fluid Dynamics ECCOMAS CFD 2010*. 2010.

[18] Kammerer, A. and Abhari, R. S. “Experimental Study On Impeller Blade Vibration During Resonance - Part 2: Blade Damping”. In: *Journal of Engineering for Gas Turbines and Power* 131.2 (2009), p. 022509. DOI: 10.1115/1.2968870.

[19] Rice, T., Bell, D., and Singh, G. “Identification Of The Stability Margin Between Safe Operation And The Onset Of Blade Flutter”. In: *Journal of Turbomachinery* 131.1 (2009), p. 011009. DOI: 10.1115/1.2812339.

[20] Carassale, L., Marrè-Brunenghi, M., and Patrone, S. “Wavelet-based identification of rotor blades in passage-through-resonance tests”. In: *Mechanical Systems and Signal Processing* 98 (2018), pp. 124–138. DOI: 10.1016/j.ymssp.2017.04.023.